

Pressure Adaptive Honeycomb: A New Adaptive Structure for Aerospace Applications

Roelof Vos^{a,b} and Ron Barrett^a

^a Department of Aerospace Engineering, The University of Kansas, Lawrence, KS, USA

^b Faculty of Aerospace Engineering, Delft University of Technology, Delft, The Netherlands

Keywords: Pressure, Adaptive, Honeycomb, morphing, aircraft, pneumatic, inflatable

ABSTRACT

A new type of adaptive structure is presented that relies on pressurized honeycomb cells that extend a significant length with respect to the plane of the hexagons. By varying the pressure inside each of the cells, the stiffness can be altered. A variable stiffness in combination with an externally applied force field results in a fully embedded pressure adaptive actuator that can yield strains well beyond the state-of-the-art in adaptive materials. The stiffness change as a function of the pressure is modeled by assigning an equivalent material stiffness to the honeycomb walls that accounts for both the inherent material stiffness as the pressure-induced stiffness. A finite element analysis of a beam structure that relies on this model is shown to correlate well to experimental results of a three-point bend test. To demonstrate the concept of embedded pressure adaptive honeycomb, an wind tunnel test article with adaptive flap has been constructed and tested in a low speed wind tunnel. It has been proven that by varying the cell pressure the flap changed its geometry and subsequently altered the lift coefficient.

NOMENCLATURE

E	Young's modulus, N/m ²
\bar{E}	Overall stiffness modulus, N/m ²
l	Wall length, m
m	mass, kg
p	Pressure, N/m ²
R	Specific gas constant, J/kg/K
t	Wall thickness, m
T	Temperature, K
θ	Honeycomb angle, deg
σ	stress, N/m ²

Subscripts and superscripts

eq	equivalent
i	initial
m	mass
p	pressure-induced
v	volume
x	longitudinal direction
y	lateral direction

Send correspondence to Roelof Vos
E-mail: r.vos@tudelft.nl

Abbreviations

CDP	Cell Differential Pressure
DARPA	Defence Advanced Research Projects Agency
FE	Finite Element
SMA	Shape Memory Alloy

1. INTRODUCTION

For more than a century, aircraft have benefitted from changes in wing geometry to account for variable flight conditions or for flight control. Although early incarnations of continuous wing deformation were quickly replaced by discrete high-lift devices and hinged control surfaces, a renewed interest in wing morphing has resulted in new implementations of this relatively old technology. In the 1980s the mission adaptive wing (MAW) explored the effectiveness of continuous leading and trailing edge deformation. This wing had an internal mechanism to flex the outer wing skin and produce a symmetrical section for supersonic speeds, a supercritical section for transonic speeds, and a high-camber section for subsonic speeds. Flight tests demonstrated that an improvement in lift-to-drag ratio of 20% could be obtained in large parts of the flight envelope while some parts even showed an increase of 100%.¹⁻⁴ Even though the flight tests demonstrated advantages of wing morphing, there were significant drawbacks to the way the morphing was achieved. Bulky, heavy hydraulic screw jacks were employed to induce the deformation in the wing. In addition, internal mechanisms employing multiple linkages ensured the desired kinematics of the mechanism. This resulted in a relatively heavy and complex actuation system. As with so many wing morphing mechanisms, comparatively small, powerful actuators imparted forces and motions to small sections which were then distributed to the larger surface. The weight increments associated with such a system clearly proved prohibitive.

Other, contemporary endeavors are under way in military aircraft, where wing morphing is applied to satisfy various mission requirements such as loiter and high-speed dash. One morphing concept relies on the simultaneous change in wing sweep, aspect ratio and span (see Fig. 1(a)). This is achieved by a scissor-link mechanism inside the wing in combination with an elastic skin.⁵ Another morphing concept folds part of the wing against the side of the fuselage, such as to reduce the total wetted area of the wing during high-speed dash (see Fig. 1(b)). In the latter approach the wing hinges are locally covered with a flexible membrane wing skin.⁶ Both of these morphing concepts have been tested in the wind tunnel and have demonstrated promising results. One of the main drawbacks for both concepts is the level of complexity that is required to achieve wing morphing. For instance, the scissor link structure consists of a complicated mechanism of hinging spars and ribs that are all interconnected. The folding wing requires individual hinges at the root and mid-span of the wing that must be able to carry the wing bending moment. In addition to the added complexity, this also must add considerable weight to an otherwise relatively lightweight wing structure.

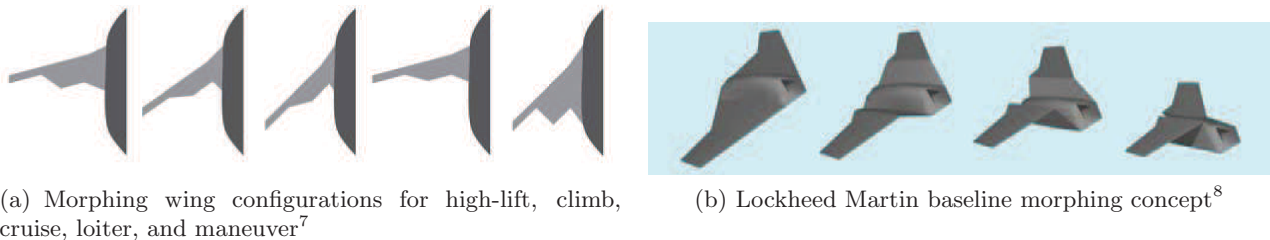


Figure 1. Contemporary morphing Concepts

In an effort to reduce the complexity of the morphing wing system, adaptive actuators were introduced to actively change (part of) the wing structure. The DARPA smart wing program utilized shape-memory-alloy (SMA) wires and torque tubes to induce various wing deformations, such as local trailing edge camber, to optimize the spanwise twist distribution.^{9,10} In 2005, Boeing introduced a higher level of adaptivity when it flew

its SMA-actuated chevrons. These chevrons, designed to reduce noise levels during take-off and landing, were slightly bent into the exhaust of the engine. At elevated altitude the decreasing local temperature caused the SMA actuators to deform such that the chevrons opened up, increasing the efficiency of the engine.¹¹ Even though this demonstrated the effectiveness of SMA actuators in civil aircraft structures, application of adaptive materials in primary and secondary structure is still prohibited due to the lack of a documented material database.

Because of the restricted use of smart materials in primary and secondary aircraft structure, a new type of adaptive structure based on ordinary honeycomb cells was developed. In this article it is shown that by pressurizing honeycomb cells, its stiffness can be altered, which can subsequently be used to induce large structural deformations. The best way of explaining the mechanics of this structure is by considering Figure 2. The test article presented in this figure consists of 23 honeycomb cells, each occupied with an airtight pouch. The cells extend a significant length (30cm) with respect to the plane of the honeycomb cells. When deflated (Fig. 2(a)) the stiffness of the honeycomb is relatively low, such that the external load (in the form of a weight) compresses the structure. By increasing the pressure in each of the pouches, the stiffness of the structure increases dramatically. This results in a structure that, under the external load, displays only little deformation. In other words, altering the pressure can alter the external geometry of this structure.

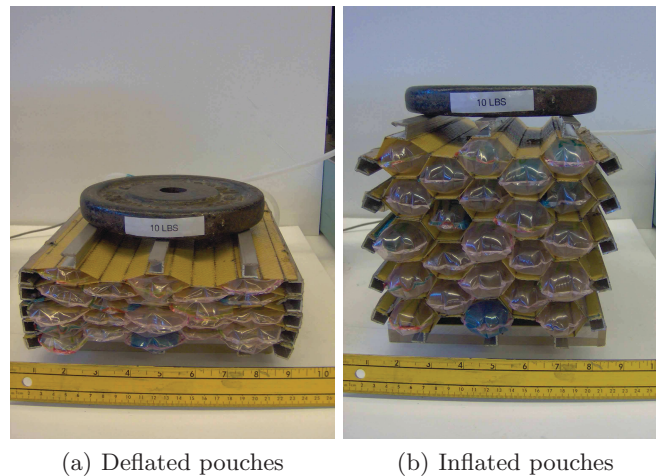


Figure 2. Proof-of-concept pressure adaptive honeycomb structure

This pressure adaptive honeycomb can be implemented in aerospace structures to locally change curvatures of components. It can be manufactured from conventional aerospace materials such as steel or aluminum and the pouches can be manufactured from an aerospace-grade of nylon. The pressurization of the pouches can be done by relying on bleed air from the compressor (in case of a jet engine) or by using the exhaust manifold pressure (in case of a propeller engine). Alternatively, the pouches can be filled with a fixed amount of air, after which they are totally sealed. In that case, the altitude-pressure relation is used as a stimulus to induce structural deformations in the pressure-adaptive honeycomb. The latter option has a higher degree of adaptivity, on the par with Boeing's variable chevrons in terms of total actuation energy density. The major differences are that all of the materials in the pressure adaptive honeycomb are immediately certifiable to FAR 23 and FAR 25 standards, they cost orders of magnitude less than SMA's and they are integrated as distributed actuators resisting distributed forces, rather than point actuators needing heavy, complicated motion distribution mechanisms.

Conventional inflatable structures have been around for several decades and have proven their applicability in aerospace structures.¹²⁻¹⁸ Partial inflation of individual cells on inflatable wings has been shown to alter airfoil geometry and change the aerodynamic characteristics.¹⁹ The only pneumatic actuator that could be qualified as an adaptive structure is a pneumatic artificial muscle that was designed to actuate a flap system.²⁰ The load-bearing capacity of honeycomb was shown for a rigidified inflatable structure. It was shown that three-dimensional honeycomb blocks could be inflated and subsequently rigidified to form walls for residential buildings. It was shown that these structures yielded low material usage, a short manufacture time, and the ability to easily

build complex structures.²¹ Other applications of (non-pressurized) honeycomb include energy absorption under in-plane compressive loading.²² Adaptive honeycomb has also been investigated where honeycombs made from SMA were used to enhance the energy absorption capability of honeycomb.²³ Even though all these research efforts have similarities to the present invention, they all differ substantially from the fundamental concept that is the topic of this paper.

2. FUNDAMENTALS OF PRESSURE ADAPTIVE HONEYCOMB

Pressure adaptive honeycomb relies on the difference in pressure between the inside of each of the cells and its surroundings. When the pressure difference between the cell and its surroundings is increased, the pressure stiffness increases accordingly. This pressure difference is generally referred to as the CDP (cell differential pressure): $CDP = p - p_a$, where p is the pressure in the cell and p_a the ambient pressure. Whether using the powered approach (controlling p) or relying on the change in ambient pressure (p_a), the geometric properties of the honeycomb pose some physical limits on the amount of shape deformation that can be achieved. Linear deformation of honeycombs is quite straightforward. Whether using the auxetic, regular or hybrid honeycomb, the longitudinal strain is independent of the number of cells that are stacked. The absolute change in dimension as a result of strain is linearly related to the strain of one individual cell. Figure 2 gives an impression of how the lateral strain exceeds -60% with respect to its inflated geometry when a CDP is applied to the pouches. Linear actuation is one of the possible applications of pressure adaptive honeycomb.

In Table 1 three possible deformation schemes are presented for a simplified honeycomb cell consisting of rigid walls connected by hinges. In the first column the perfect hexagon is shown. This is the shape the honeycomb takes when an infinite CDP is present. In the second column the deployed shape of the honeycomb is displayed. This is the shape the honeycomb cells would ideally take when no CDP (Δp) is applied. Next to that are the maximum strains in longitudinal (x) and lateral (y) direction. With global strains being defined as:

$$\varepsilon_x = \frac{x_0 - x_1}{x_0} = \frac{\cos \theta - \sin \theta_i}{\sin \theta_i} \quad \varepsilon_y = \frac{y_0 - y_1}{y_0} = \frac{\sin \theta - \cos \theta_i}{1 + \cos \theta_i} \quad (1)$$

where θ is the honeycomb angle (see Table 1) and θ_i the initial honeycomb angle in the unstrained position. The honeycomb angle is the angle measured between the diagonal member and the horizontal and is denoted with θ . The change in honeycomb angle, $\Delta\theta$ is a good indication for the amount of bending that the walls of the honeycomb cells need to sustain in order to deform between the two given shapes.

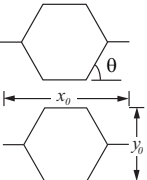
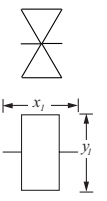
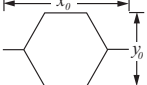
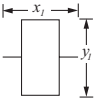
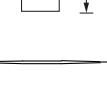
Table 1 displays the maximum strains that the honeycomb experiences during its transformation between the two shapes. The strain is measured with respect to the dimensions of the honeycomb when its cells form perfect hexagons (as in the first column). The final column displays the change in honeycomb angle, θ that is required to attain this amount of strain. From the data of Table 1 it can be seen that the most linear displacement in x direction can be found when the honeycomb changes between the auxetic shape and the regular shape. A potential disadvantage for this shape is the fact that the strain in y direction changes sign during deformation. When a small amount of bending is required in the honeycomb (to prevent any plastic deformation, for example) it can be wise to limit the change in honeycomb angle and have a shape change between rectangular and hexagonal honeycomb.

The deformation shown in the bottom row of Table 1 is similar to the one shown in Figure 2. There is a potential for very high lateral deformation. Apart from linear deformation, pressurized honeycomb can be used to induce changes in curvature when it is bounded on one side to a plate. A schematic example of how this can be achieved is shown in Figure 3. Here, a rectangular honeycomb is used as the cell that borders the free boundary. This results in a convex shape of the curved plate.

3. THEORETICAL AND EXPERIMENTAL CHARACTERIZATION

To predict the mechanical behavior of pressure-adaptive honeycomb under loading an analytical model has been developed that translates the structural stiffness of the pressurized honeycomb structure to an equivalent Young's modulus of the cell walls. An FE model of a honeycomb beam structure that relies on this equivalent Young's modulus has been correlated to experimental results, obtained from a three-point bend test of a pressurized honeycomb beam.

Table 1. Geometric properties of pressure adaptive honeycomb

CDP = ∞	CDP = 0	$(\varepsilon_x)_{max}$	$(\varepsilon_y)_{max}$	$\Delta\theta$ (rad)
		-67%	$\pm 15\%$	$\pi/3$
		-33%	+15%	$\pi/6$
		+33%	-100%	$\pi/3$

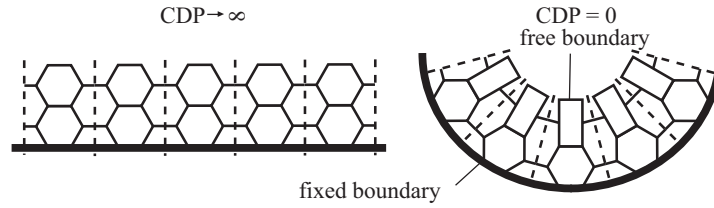


Figure 3. Example of a curvature change due to pressure adaptive honeycomb

3.1 Analytical Modeling of Pressure Adaptive Honeycomb

The global stiffness of pressurized honeycomb is determined by two factors: the material-induced stiffness and the pressure-induced stiffness. The material-induced stiffness is a function of the honeycomb material (i.e. its Young's modulus, E^m), and its geometric properties. It has been shown that for honeycomb where all cell walls have a uniform thickness-to-length ratio (t/l) the material-induced stiffness (\bar{E}^m) can be related to the Young's modulus according to:²⁴

$$\bar{E}_x^m = E^m \left(\frac{t}{l} \right)^3 \frac{\cos \theta_i + 1}{\sin^3 \theta_i} \quad \text{and} \quad \bar{E}_y^m = E^m \left(\frac{t}{l} \right)^3 \frac{\sin \theta_i}{(1 + \cos \theta_i) \cos^2 \theta_i} \quad (2)$$

where θ_i is the initial honeycomb angle.

To determine the pressure-induced stiffness of the pressurized honeycomb, a constant energy approach can be taken where the externally applied work on the structure, W_{ex} , equals the useful work, W_{use} , carried out by the pressurized volume. In their most general form, the expression for the external and useful work read:

$$W_{use} = \int_{V_i}^V p dV - p_a(V - V_i) \quad \text{and} \quad W_{ex} = \int_s F ds \quad (3)$$

The force, F , can be related to the stress, σ , while the displacement, s can be related to the overall strain, ε (see also Table 1. In addition, the volume, V can be related to the honeycomb angle, θ , which can also be related to the overall strain (Eq. 1). By assuming that $W_{use} = W_{ex}$ it is therefore possible to state an explicit relationship between the stress in principal directions and the honeycomb angle. In the case the pressure in the pouches is kept constant this relationship can be written according to:

$$\sigma_x = \frac{1}{l^2(1 + \cos \theta_i)} \times \frac{(p - p_a)(V - V_i)}{\sin \theta - \sin \theta_i} \quad \text{and} \quad \sigma_y = \frac{1}{l^2 \sin \theta_i} \times \frac{(p - p_a)(V - V_i)}{\cos \theta - \cos \theta_i} \quad (4)$$

In the the pouches are completely sealed and the mass, m , inside the pouches remains constant, this relationship yields:

$$\sigma_x = \frac{1}{l^2(1 + \cos \theta_i)} \times \frac{mRT \ln(V/V_i) - p_a(V - V_i)}{\sin \theta - \sin \theta_i} \quad \text{and} \quad \sigma_y = \frac{1}{l^2 \sin \theta_i} \times \frac{mRT \ln(V/V_i) - p_a(V - V_i)}{\cos \theta - \cos \theta_i} \quad (5)$$

where R is the specific gas constant of the gas inside the pouches, while T is the temperature of air inside the pouches (assumed constant).

From the parametric stress-strain relationship the pressure-induced stiffness, \bar{E}^p can be calculated by employing the chain rule:

$$\bar{E}_x^p = \frac{d\sigma_x}{d\varepsilon_x} = \frac{\sigma_x}{d\theta} \frac{d\theta}{d\varepsilon_x} \quad \text{and} \quad \bar{E}_y^p = \frac{d\sigma_y}{d\varepsilon_y} = \frac{\sigma_y}{d\theta} \frac{d\theta}{d\varepsilon_y} \quad (6)$$

. The superposition of the material-induced stiffness and the pressure-induced stiffness yields the global stiffness of the pressurized honeycomb:

$$\bar{E}_x = \bar{E}_x^m + \bar{E}_x^p \quad \text{and} \quad \bar{E}_y = \bar{E}_y^m + \bar{E}_y^p \quad (7)$$

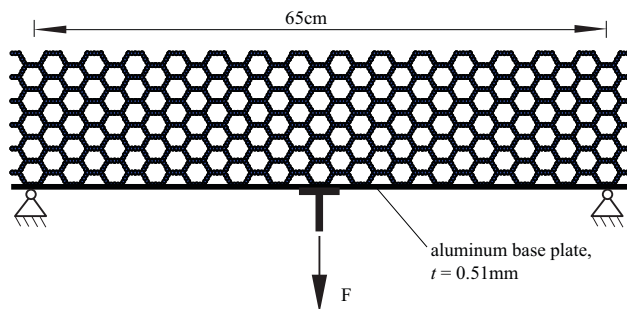
To use this analytical model in a finite element approximation it is convenient to map the overall stiffness of the pressurized honeycomb onto the honeycomb material. This allows the designer to solely model the honeycomb grid without the addition of pressurized pouches, the interaction between pouch and cell wall, or the pressure inside the pouch. The Young's modulus of a honeycomb structure that possesses the same kinematic and stiffness properties (i.e. with an equivalent Young's modulus, E^{eq}) as its pressurized equivalent can be found by applying Eq. 2 inversely:

$$E^{eq} = \bar{E}_x \left(\frac{l}{t}\right)^3 \frac{\sin^3 \theta_i}{\cos \theta_i + 1} \quad \text{or} \quad E^{eq} = \bar{E}_y \left(\frac{l}{t}\right)^3 \frac{(1 + \cos \theta_i) \cos^2 \theta_i}{\sin \theta_i} \quad (8)$$

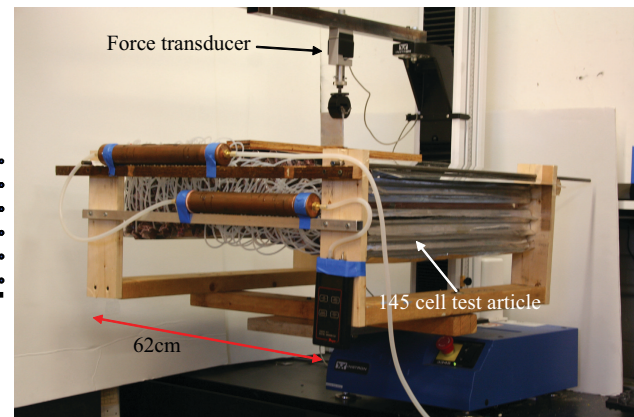
An elaborated discussion of the theory that has been presented in this section can be found in Vos, 2009.²⁵

3.2 Experimental Testing and Results

To investigate the validity of the equivalent-stiffness model a three-point bend test was carried out on a 145-cell pressurized honeycomb beam. This beam measured 65cm in span and the honeycomb consisted of sheet metal. As a base material for the honeycomb Aluminum 1145H19 was chosen with a thickness of 76μm. The reason for this option was that it had shown good manufacturability properties in the sense that it allowed for straight folds to be induced by a simple press brake. In addition, it had relatively high yield strength, which was important because it needed to stay in the elastic realm while deforming. The aluminum sheets were cut, folded, and bonded together using Hysol 9412. The face length of a characteristic cell measured $l = 15\text{mm}$. To accommodate this rather large test article, a frame was built that could be mounted to the base of the Instron Machine. A schematic representation of the test is shown in Figure 4 along with an image of the physical test setup.



(a) Schematic representation of three-point bend test on 145-cell pressure adaptive honeycomb



(b) Photo of experimental setup in Instron 3345

Figure 4. A three-point bend test was carried out to compare to results from FE calculations

An FE analysis was carried out by relying on the equivalent stiffness approach (Eq. 8) in combination with an invariable pressure differential. In addition, a linearization was applied to the stress-strain relationship (Eq. 4) to ensure a constant equivalent Young's modulus for the testing pressures ($p = 10\text{kPa}$ and $p = 20\text{kPa}$, respectively). The FE program Finesse was used to resolve the displacements of the structure as a function of the force applied in the center of the base plate. These displacements were subsequently compared to the real displacements at these forces that were recorded during the experiment.

From Figure 5 it can be observed that the correlation of the experimental results to the FE-generated results is very good. From these experiments it can be concluded that the finite element analysis with the analytically obtained Young's modulus gives a good approximation of the mechanics of pressure adaptive honeycomb and can be used with confidence in a finite element analysis of more complicated geometries. For more elaborate test results the reader is referred to Vos, 2009.²⁵

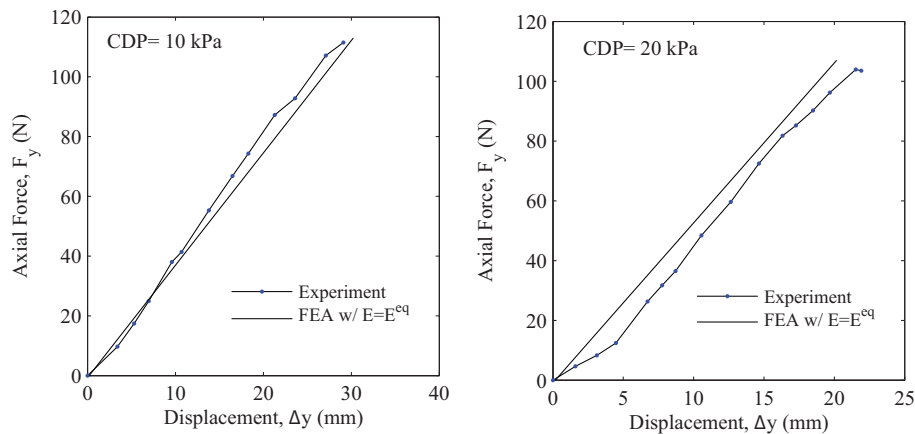


Figure 5. Results of three-point bend test and correlation to FE results

4. COMPARISON TO ADAPTIVE MATERIALS

In the previous section it has been demonstrated that with a simple analytical approximation of the equivalent stiffness, it is possible to model the mechanical properties of the pressure adaptive honeycomb. It has also been shown in Table 1 that pressure adaptive honeycomb can potentially exhibit very large strains. In this section the pressure-adaptive honeycomb is perceived as an adaptive actuator and is compared to adaptive materials in terms of mass-specific and volume-specific energy density. To that extent a more realistic representation of the honeycomb cell is considered where the bending of the walls is representative for the amount of strain that can be achieved. In Figure 6 these maximum strains are schematically depicted for a single honeycomb cell. It is assumed that the honeycomb cell is manufactured, such that its geometry does not form a regular honeycomb, but has a honeycomb angle other than 60° (center cell). Application of external loading results in a deformation of the cell (right cell), while the application of a cell differential pressure (CDP) results in a shape which is close to a perfect regular hexagon. The strains in this figure are all measured with respect to the regular hexagonal geometry and are based on the assumptions laid out by Gibson and Ashby²⁴ for thin-walled honeycomb cells.

To compare the present adaptive structure to existing adaptive actuator elements, the assumption has been made that the atmospherically-induced pressure adaptive structure would encounter a 40kPa pressure difference between take-off and cruise altitude and that a high-pressure compressor of a typical contemporary jet engine could produce a 0.9MPa CDP. Based on these numbers the maximum blocked stress and free strain have been calculated using an analytical model based on analytical model of the previous section. The resulting properties are summarized in Table 2.

In a study carried out by SRI and DARPA,²⁶ a variety of active materials were investigated such that their overall characteristics could be easily compared. Based on the characteristics of pressure adaptive honeycomb (Table 2) and the data from the aforementioned reference Figure 7 compares the volumetric energy density of this

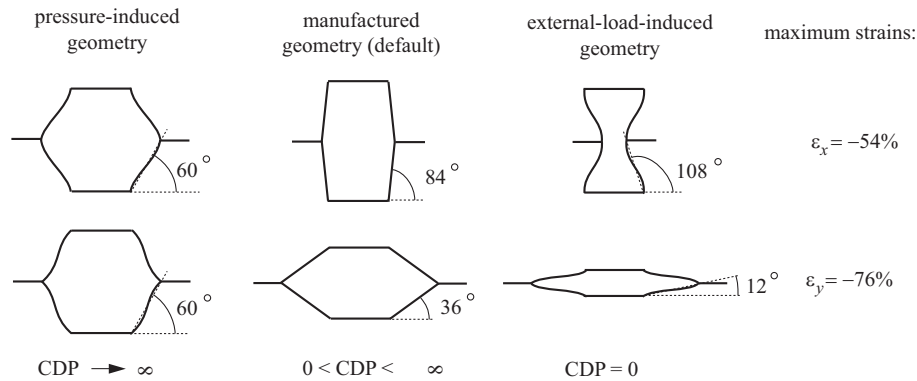


Figure 6. Maximum strains in longitudinal (x) and lateral (y) direction with no plastic deformation in the cell walls, based on the assumption of a small thickness-to-length ratio of the cell wall ($t/l < 1/4$).

Table 2. Characteristics of two types of pressure adaptive honeycomb.

Actuator Type (specific example)	Maximum Strain, ϵ (%)	Maximum Pressure, σ (MPa)	Specific Elastic Energy Density, E_m (J/g)	Elastic Energy Density, E_v (J/cm ³)	Transfer Efficiency, η (%)	Maximum Efficiency, η (%)	Specific Density, ρ (g/cm ³)	Relative Speed (full cycle)
Pressure Adaptive Honeycomb								
Atmospherically-Triggered	76	0.07	1.1	0.027	100	n/a	0.025	slow
High-Pressure (0.9MPa)	76	0.82	12.4	0.31	~95	n/a	0.025	slow

adaptive structure to other active materials. It can be seen from this figure that pressure adaptive honeycomb belongs to the group of adaptive structures showing the highest strains. The volumetric energy density is on the par with PZT 5H in case of the high-pressure adaptive honeycomb.

If the volumetric energy density is divided by the material density of the active structure the mass-specific energy density is found. Comparing pressure-adaptive honeycomb to other active materials with respect to this characteristic shows that the mass-specific energy density of pressure adaptive honeycomb is on the same order of magnitude as for shape memory alloy (SMA, see Figure 8). While SMA has a comparatively low transfer efficiency ($\sim 10\%$), it can be argued that pressure-adaptive honeycomb hardly dissipates any energy. In the case of the atmospherically-triggered version, no onboard energy source is required to actuate this structure. A transfer efficiency of 100% is therefore realistic. Pressure losses between source and actuator have been estimated to account for an energy dissipation of 5% for the case of a high-pressure version of pressure adaptive honeycomb.

5. POTENTIAL APPLICATION: PRESSURE ADAPTIVE FLAP

To demonstrate the workings of pressure adaptive honeycomb in a realistic aerospace application, a wing section was constructed with a pressure adaptive flap in place. The wing section measured 91cm in chord and was modeled after a NACA 2412 airfoil. The pressure adaptive honeycomb was applied over the aft 35% of the wing chord. In each of the honeycomb cells an inflatable mylar pouch was inserted that connected to a central pressurization apparatus. The honeycomb was attached to the top skin, the trailing edge, and the wing root. The bottom skin could slide freely with respect to the trailing edge and the honeycomb. Both bottom and top skin were pre-curved, such as to ensure the increased camber over the aft part of the wing when no CDP was present. Increasing the CDP decreased the camber substantially such that an airfoil shape close to the NACA 2412 profile was obtained. In Figure 9(a) the measured outline of the wing profile is shown (under wind-off conditions). The NACA 2412 airfoil has been superimposed for reference. As can be seen from this plot, large deformations could be achieved when a CDP of 40kPa was applied. As this was a proof-of-concept test article, the exact shape of the 2412 airfoil was approximated when pressure to the cells was applied.

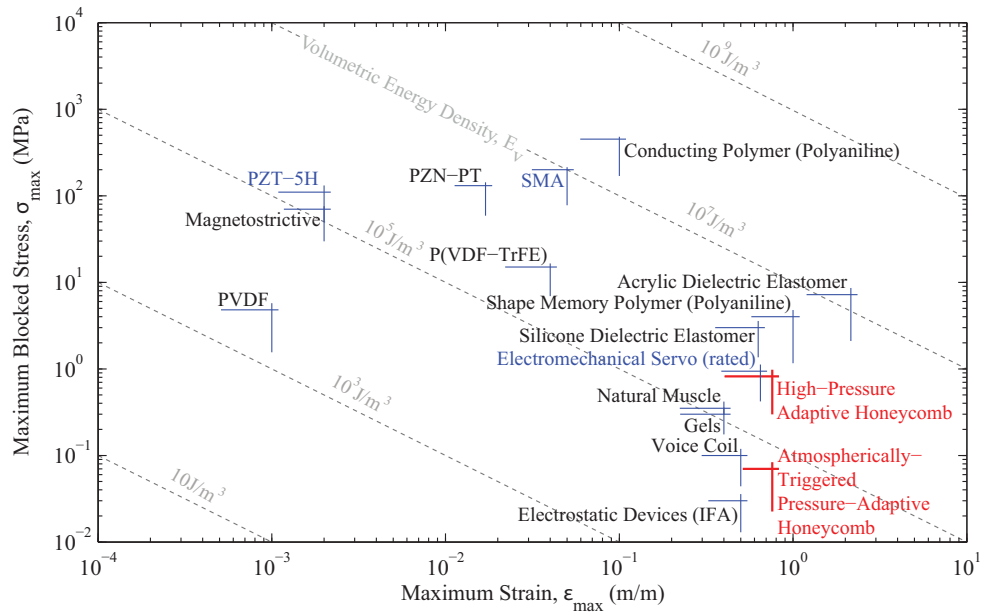


Figure 7. Comparison between two types of pressure adaptive honeycomb (atmospherically-triggered and high-pressure) to the state-of-the-art in active materials.²⁶

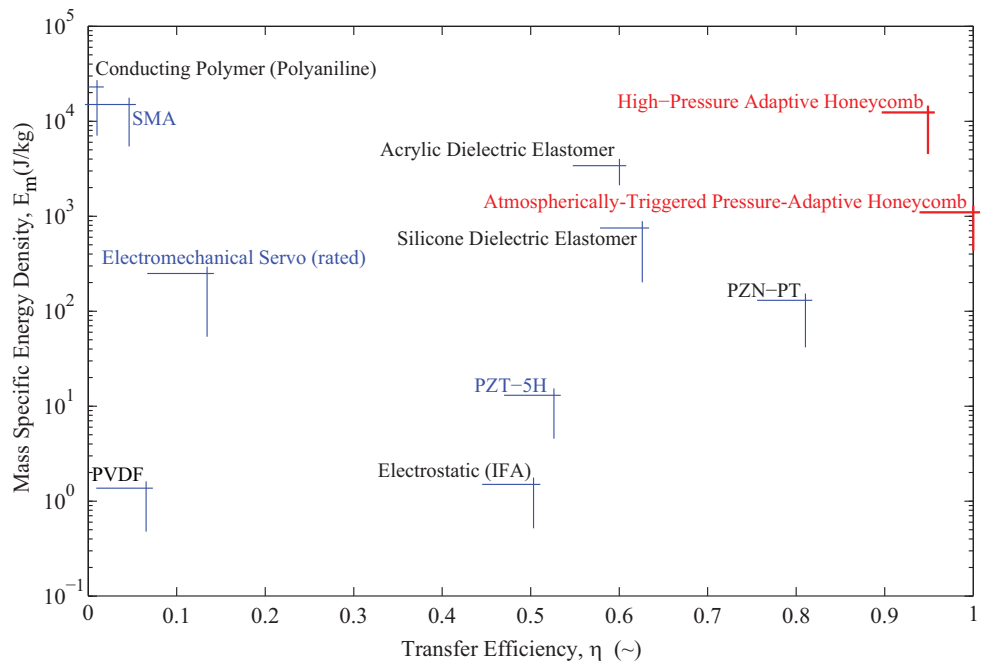
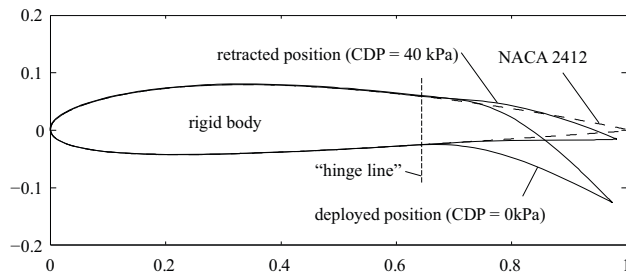
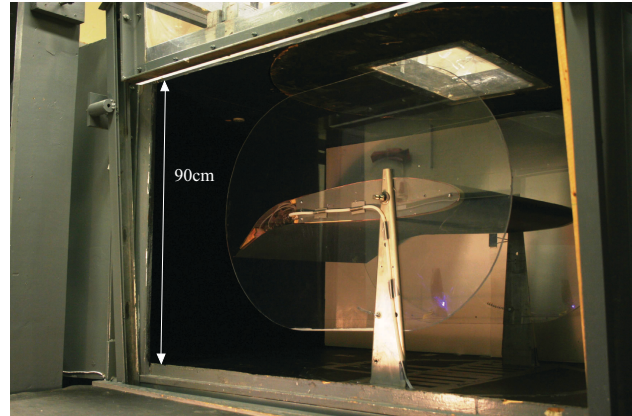


Figure 8. Comparison of mass-specific energy densities of pressure adaptive honeycomb and the state-of-the-art in active materials.^{26,26}

The test article was clamped between two transparent end plates. These end plates were put in place to minimize airflow around the wing tips. The transparency of the end plates ensured that the position of the flap could be photographed during the tests. The test article was positioned in the subsonic wind tunnel at The University of Kansas (see Figure 9(b)). A six-axes balance system connected to Labview ensured that all aerodynamic coefficients could be measured. These coefficients were subsequently corrected for the blockage



(a) Applying a CDP of 40kPa created a substantial change in airfoil camber over the aft 35% of this airfoil. In wind-off conditions. The NACA 2412 airfoil shape is superimposed for reference



(b) Wing section with pressure adaptive flap positioned in the low speed wind tunnel at The University of Kansas

Figure 9. Wind tunnel experimental test article and test setup

effects of the wind tunnel walls using the methods laid out by Barlow et al.²⁷

In Figure 10 the section lift coefficient versus the angle of attack is shown for five different values of CDP and a Reynolds number of approximately one million. It can be seen that the lift coefficient is increased by approximately 0.3 over the entire range of angles of attack when the CDP drops from 40kPa to 0kPa. This demonstrates the effectiveness of the pressure adaptive flap. A careful observer might wonder why the airfoil does not show any stall behavior. This is attributed to the wind tunnel wall effects, which were substantial (17% of area blockage). The relatively large wind tunnel model was necessary to allow for the accurate manufacturing of the honeycomb structure in the pressure adaptive flap. In future applications, it is anticipated that the honeycomb grid will form a finer maze and therefore allow for smaller test articles. For the purpose of this test, however, the pressure adaptive honeycomb demonstrated excellent performance.

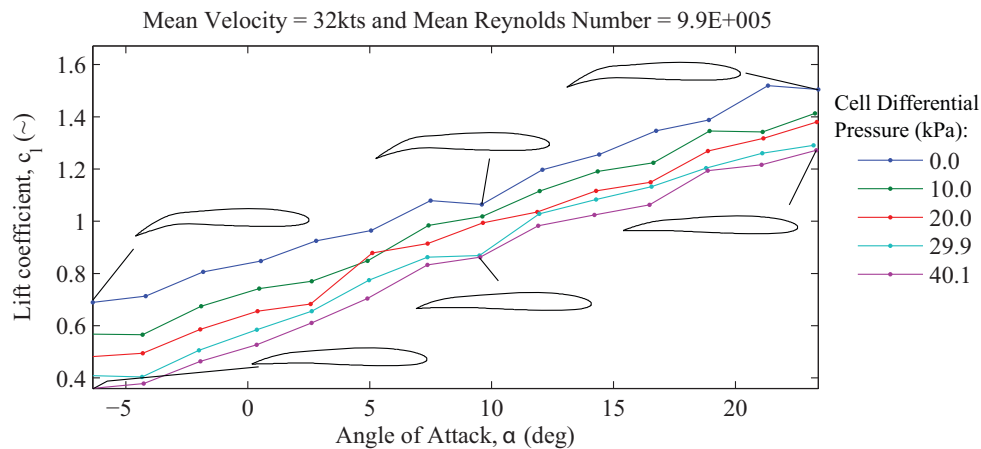


Figure 10. Section lift coefficient versus angle of attack

6. CONCLUSIONS

A new type of adaptive structure has been introduced: pressure adaptive honeycomb. It has been shown that pressure adaptive honeycomb can exhibit strains up to 100% and can therefore be beneficial to apply in morphing

aircraft structures. Estimates of the volume-specific energy density showed that pressure-adaptive honeycomb is on the par with PZT-5H ($0.31\text{J}/\text{cm}^3$), while its mass-specific density is on the par with shape memory alloy ($12.4\text{J}/\text{g}$). However, the transfer efficiency of pressure adaptive honeycomb has been shown to be substantially higher than for any of the other adaptive materials. It has been shown that an analytical model for the prediction of the equivalent stiffness of pressurized honeycomb correlates well to experimental tests. In addition, it has been demonstrated in the wind tunnel that pressure adaptive honeycomb can be successfully applied in a morphing flap structure to alter the outer shape of the wing and subsequently change the lift coefficient.

ACKNOWLEDGEMENTS

The authors wish to acknowledge the generous support of the University of Kansas Transportation Research Institute (TRI) and the Aerospace Engineering Department for funding this research. In addition, the authors wish to acknowledge the support from Prof. Karan S. Surana and Prof. Albert Romkes, Mechanical Engineering Department, University of Kansas, for providing the FE program FINESSE to perform the FE computations in this work. The authors would also like to recognize Ms. Lauren Kerth, Mr. Thomas Stastny and Mr. Ryan Barnhart for their tireless efforts in assisting fabricating the test articles.

REFERENCES

- [1] DeCamp, R. W. and Hardy, R., "Mission adaptive wing advanced research concepts," in [*A collection of Technical Papers (AIAA Atmospheric Flight Mechanics Conference)*], 465–470, American Institute of Aeronautics and Astronautics, Washington D.C. (1984).
- [2] Gould, D. K., "Mission adaptive wing flight demonstration program," in [*SAE Aerospace Congress & Exposition*], SAE-811035, Anaheim California (1981).
- [3] Lewis, G. E., Thomasson, R. E., and Nelson, D. W., "Wing lift/drag optimization system," United States Patent 4,899,284 (Feb. 6 1990).
- [4] Powers, S. G. and Webb, L. D., "Flight wing surface pressure and boundary-layer data report from the f-111 smooth variable-camber supercritical mission adaptive wing," tech. rep., NASA Technical Memorandum 4789 (June 1997).
- [5] Flanagan, J. S., Strutzenberg, R. C., Myers, R. B., and Rodrian, J. E., "Development and flight testing of a morphing aircraft, the nextgen mfx-1," in [*48th AIAA/ASME/ASCE/AHS/ASC Structures, Structural Dynamics, and Materials Conference*], AIAA Paper 2007-1707, Honolulu Hawaii (2007).
- [6] Ivanco, T. G., Scott, R. C., Love, M. H., Zink, S., and Weisshaar, T. A., "Validation of the lockheed martin morphing concept with wind tunnel testing," in [*48th AIAA/ASME/ASCE/AHS/ASC Structures, Structural Dynamics, and Materials Conference*], AIAA Paper 2007-2235, Honolulu, Hawaii (2007).
- [7] Bowman, J., Sanders, B., Cannon, B., Kudva, J., Joshi, S., and Weisshaar, T., "Development of next generation morphing aircraft structures," in [*48th AIAA/ASME/ASCE/AHS/ASC Structures, Structural Dynamics, and Materials Conference*], AIAA Paper 2007-1707, Honolulu, Hawaii (2007).
- [8] Love, M., Zink, P., Stroud, R., Bye, D., Rizk, S., and White, D., "Demonstration of morphing technology through ground and wind tunnel tests," in [*48th AIAA/ASME/ASCE/AHS/ASC Structures, Structural Dynamics, and Materials Conference*], AIAA Paper 2007-1729, Honolulu, HI (2007).
- [9] Sanders, B., Cowan, D., and Scherer, L., "Aerodynamic performance of the smart wing control effectors," *Journal of Intelligent Material Systems and Structures* **15**, 293–303 (2004).
- [10] Martin, C. A., Hallam, B. J., Flanagan, J. S., and Bartley-Cho, J., "Design, fabrication, and testing of a scaled wind tunnel model for the smart wing project," *Journal of Intelligent Material Systems and Structures* **15**, 269–278 (2004).
- [11] Calkins, F. T. and Butler, G. W., "Variable geometry chevrons for jet noise reduction," in [*12th AIAA/CEAS Aeroacoustics Conference*], AIAA Paper 2006-2546, Cambridge, Massachusetts (2006).
- [12] Cadogan, D., Smith, T., Uhelsky, F., and MacKusick, M., "Morphing inflatable wing development for compact package unmanned aerial vehicles," in [*45th AIAA/ASME/ASCE/AHS/ASC Structures, Structural Dynamics and Materials Conference*], AIAA 2004-1807, Palm Springs, CA (2004).
- [13] Norris, R. K. and Pulliam, W. J., "Historical perspective on inflatable wing structures," in [*50th AIAA/ASME/ASCE/AHS/ASC Structures, Structural Dynamics, and Materials Conference*], (2009).

- [14] Sebrell, W. A., "Inflatable wing," United States Patent 3,957,232 (May 18 1976).
- [15] Priddy, T. G., "Inflatable wing," United States Patent 7,725,021 (Feb. 16 1988).
- [16] Ritter, D. L., "Light weight pneumatic airplane," United States Patent 2,886,265 (May 12 1959).
- [17] Bain, B. K., "Inflatable airplane," United States Patent 3,106,373 (Oct. 8 1963).
- [18] Chutter, R. R., "Pneumatic tubular construction," United States Patent 3,473,761 (Oct. 21 1969).
- [19] Reinhard, A., To, F. E., Ramseier, O., and Kammer, R., "Adaptive pneumatic wing for fixed wing aircraft," United States Patent 6,199,796B1 (Mar. 13 2001).
- [20] Woods, B., Bubert, E., Kothera, K., and Wereley, N., "Design and testing of a biologically inspired pneumatic trailing edge flap system," in [*49th AIAA/ASME/ASCE/AHS/ASC Structures, Structural Dynamics, and Materials Conference*], AIAA, Schaumburg, IL (2008).
- [21] Khire, R. A., Dessel, S. V., Messac, A., and Mullur, A. A., "Study of a honeycomb-type rigidified inflatable structure for housing," *Journal of Structural Engineering* **132**(10), 1664–1672 (2006).
- [22] Atli, B. and Gandhi, F., "Energy absorption of cellular honeycombs with various cell angles under in-plane compressive loading," in [*49th AIAA/ASME/ASCE/AHS/ASC Structures, Structural Dynamics, and Materials Conference*], (2008).
- [23] Shaw, J. A., Churchill, C., Grummon, D., Triantafyllidis, N., Michailidis, P., and Foltz, J., "Shape memory alloy honeycombs: experiments & simulation," in [*48th AIAA/ASME/ASCE/AHS/ASC Structures, Structural Dynamics, and Materials Conference*], (2007).
- [24] Gibson, L. J. and Ashby, M. F., [*Cellular Solids, Structure and Properties*], Cambridge University Press, 1 ed. (1988).
- [25] Vos, R., *Mechanics and Applications of Pressure Adaptive Honeycomb*, ph.d. thesis, The University of Kansas, Department of Aerospace Engineering, Lawrence, KS (September 2009).
- [26] Anon., "Comparison of eaps with other actuator technologies," in [*ndea.jpl.nasa.gov/nasande/lommas/eap/*], SRI International and DARPA (Accessed: May 30 2009).
- [27] Barlow, J. B., Rae, W. H., and Pope, A., [*Low-Speed Wind Tunnel Testing*], Wiley & Sons, New York, 3 ed. (1999).